*The Canadian Mineralogist*
Vol. 31, pp. 727-744 (1993)

# NOTEWORTHY MINERALOGY OF THE Au–Ag–Sn–W(Bi) EPITHERMAL ORE DEPOSIT OF CIROTAN, WEST JAVA, INDONESIA

ERIC MARCOUX AND JEAN-PIERRE MILÉSI

*Bureau de Recherches Géologiques et Minières, B.P. 6009, 45060 Orléans Cedex 2, France*

SIMPWEE SOHEARTO AND RUSMAN RINAWAN

*Direktorat Sumberdaya Minerals, 57 Jalan Diponegoro, Bandung 40122, Indonesia*

## ABSTRACT

The Cirotan Au–Ag ore deposit (Java, Indonesia), of Pliocene age (1.7 ± 0.1 Ma), is a particular type of "adularia–sericite" epithermal deposit. The polymetallic paragenesis begins with a fairly classic epithermal association of pyrite–marcasite (pseudomorphs after pyrrhotite), galena, sphalerite, rare chalcopyrite and arsenopyrite in a quartz – sericite – rhodochrosite (± rhodonite) gangue. Then, as the mineralized structure developed, the paragenesis evolved progressively to an unusual mineralogy with, in particular, the appearance of Zn-bearing greenockite (up to 6.5 wt.% Zn), uytenbogaardtite ($Ag_3AuS_2$), Te-bearing canfieldite ($Ag_8SnTe_2S_4$), Ag–Bi-rich lillianite ($AgPb_4Bi_5S_{12}$) and abundant cassiterite, ferberite (88–92 mole % $FeWO_4$) and scheelite. At the same time, electrum, which in the early stages is rare (<2 g/t Au), in small grains (<10 μm) and silver rich (26–48 wt.% Ag), became abundant (as much as 400 g/t Au), the grains larger (up to 230 μm) and richer in gold (10–38 wt.% Ag). This paragenesis reflects an evolution in conditions of deposition toward lower $f(S_2)$ at a temperature (according to evidence from the fluid inclusions) of around 250°C. These later minerals are typical of deposits close to a magma source and are very rare in epithermal deposits. Cirotan may therefore be considered as a hybrid deposit transitional between the low-level adularia–sericite epithermal type and the porphyry-tin type of deposit.

*Keywords:* epithermal, Java, Indonesia, cassiterite, ferberite, gold, Te-bearing canfieldite, lillianite, uytenbogaardtite, hybrid deposit.

## SOMMAIRE

Le gisement Au–Ag pliocène (1,7 ± 0,1 Ma) de Cirotan (Java occidental, Indonésie) est un type particulier de gîte épithermal à adulaire–séricite. La paragenèse polymétallique est assez classique au départ: pyrite – marcasite en pseudomorphose de pyrrhotite, galène, sphalérite, chalcopyrite et arsénopyrite rares, dans une gangue de quartz – séricite – rhodochrosite (± rhodonite). Elle évolue progressivement vers une minéralogie originale au fur et à mesure que la structure minéralisée se façonne, avec notamment l'apparition de greenockite zincifère (jusqu'à 6,5 % pds Zn), de uytenbogaardtite ($Ag_3AuS_2$), de canfieldite à tellure ($Ag_8SnTe_2S_4$), de lillianite riche en Ag–Bi ($AgPb_4Bi_5S_{12}$) et d'abondantes cassitérite, ferbérite (88–92 mole % $FeWO_4$) et scheelite. Parallèlement, l'électrum, d'abord rare (<2 g/t Au), en grains fins (<10 μm) et riche en argent (26–48 % pds Ag), devient abondant (jusqu'à 400 g/t Au), en grains grossiers (50–230 μm) et plus riche en or (10–38 % pds Ag). Cette paragenèse traduit une évolution du dépôt vers des conditions de plus faible $f(S_2)$ sous une température, fixée par les inclusions fluides, d'environ 250°C. Ces minéraux sont typiques des gîtes proches de leur magma-source et sont très rares dans les gîtes épithermaux. Le gisement de Cirotan peut être considéré comme un gisement hydride, intermédiaire entre le type adulaire–séricite classique et le type des porphyres stannifères.

*Mots-clés:* épithermal, Java, Indonésie, cassitérite, ferbérite, électrum, canfieldite à tellure, lillianite, uytenbogaardtite, gisement hybride.

## INTRODUCTION

The official production of gold from primary gold deposits in Indonesia between 1899 and 1989 was 180 t (Sunarya 1989), almost entirely obtained from Miocene–Pliocene epithermal veins. Present Indonesian gold production (4.73 t/yr) comes mainly from three mines: Tembagapura in Irian Jaya (3.72 t/yr), Lebong Tandai (0.77 t/yr) and Cirotan (0.16 t/yr) (1988 production figures given by MacDivitt 1990). The Cirotan mine, the main gold-producing center of the Cikotok district and of the island of Java, produced 7.6 t Au and 193 t Ag between 1955 and 1991 (Sunarya 1989; Aneka Tambang, written comm.) and

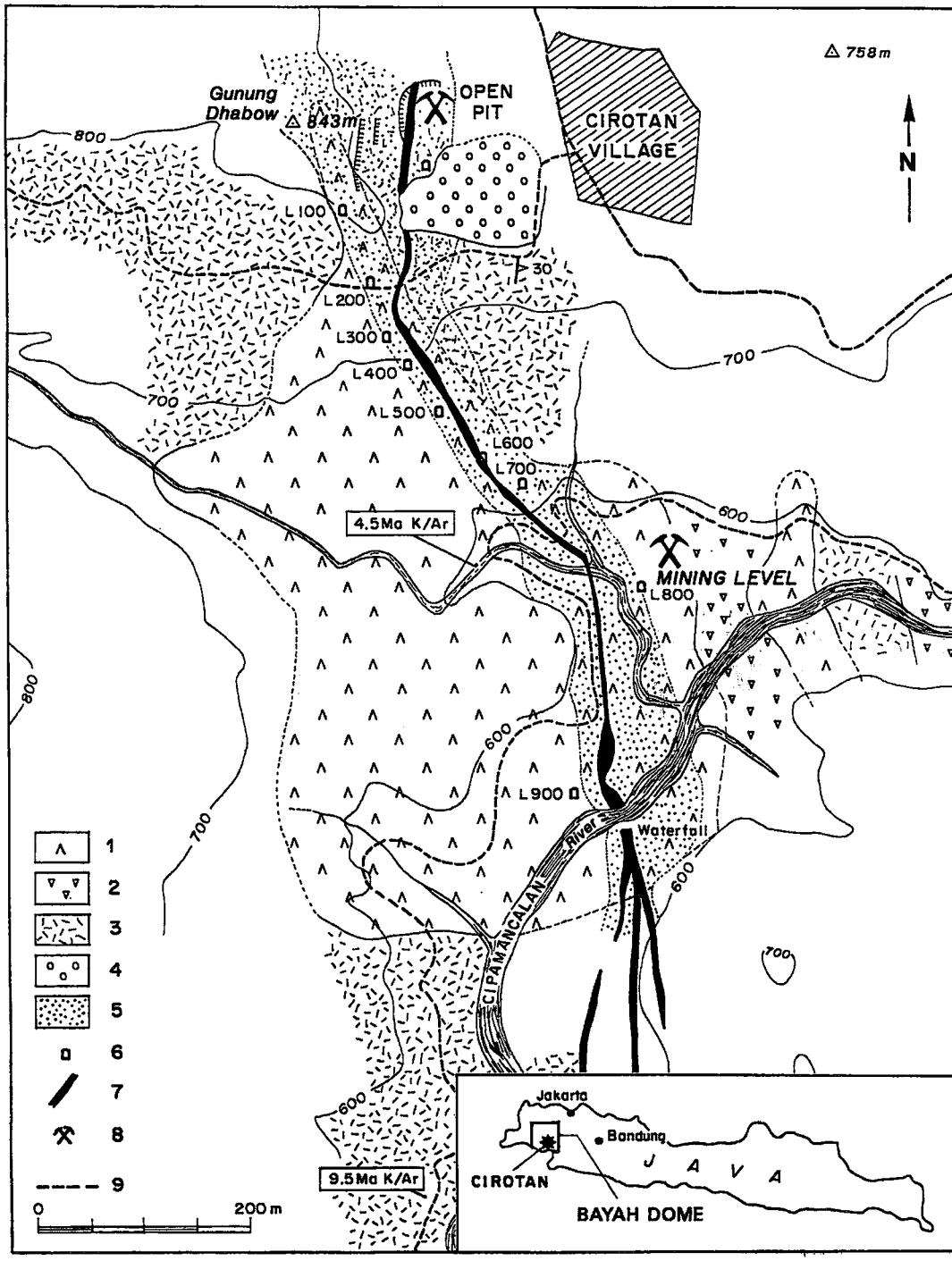


FIG. 1. Location and geological map of Cirotan. Symbols: 1 Microdiorite (4.5 Ma), 2 Andesites (9.0 to 14.5 Ma), 3 Rhyolitic ignimbrites (9.5 Ma), 4 Mud flow, 5 Silicification halo, 6 Gallery, 7 Cirotan ore deposit, 8 Exploitation levels (1991), 9 Road.

has an annual production of about 0.2 t Au, 3 t Ag, 500–700 t Zn concentrates and 150–220 t Pb concentrates (Aneka Tambang, written comm.).

The study of the Cirotan mine has revealed a noteworthy mineralogical association marked by (a) the appearance, toward the end of the mineralization, of wolframite associated with cassiterite, a mineral not previously reported in Pacific Rim epithermal deposits, and (b) several rare mineral species, such as uytenbogaardtite, Te-bearing canfieldite, Zn-bearing greenockite, and a Ag–Bi-rich variety of lillianite. In this article, we will describe the mineralogy of the Cirotan deposit, with emphasis on those mineralogical and textural features that add to our knowledge of Pacific Rim epithermal gold deposits.

## Geological Setting

The Cirotan deposit (Fig. 1), along with other gold deposits, lies within the Bayah dome, a Tertiary–Quaternary volcanic structure of about 30 × 30 km in the southwestern part of the island of Java (southwest of Jakarta Province), which forms part of the Sunda Arc. The Bayah dome is composed of Oligocene–Miocene to Pliocene–Quaternary calc-alkaline rhyolitic to calc-alkaline andesitic intrusive rocks, with horizons of Miocene limestone and sandstone in its southern part (Van Bemmelen 1949; DSM/BRGM written comm. 1991); several authors have shown that the volcanism has migrated from south to north with time (Katili 1975, Whitford *et al.* 1979, Claproth 1989). The gold deposits of the Bayah dome lie within a general north–south belt, and some can be interpreted as megatension cracks resulting from N–S to N20°E compression related to subduction beneath the island of Java.

The Cirotan structure (Fig. 1), 1350 m long and as much as 25–30 m thick, strikes N170°E and dips 50–60°E. It cuts a body of quartz microdiorite (dated at 4.5 ± 0.3 Ma by the K/Ar method; Milési *et al.*, in press) intrusive in a thick rhyodacitic to andesitic ignimbrite complex of Middle to Late Miocene age (K/Ar dates of 9.5 to 14.3 Ma); the structure has been dated at 1.7 ± 0.1 Ma (K/Ar method on orthoclase of adularia habit; Milési *et al.*, in press). Structural studies have shown that the mineralized structure is a dextral strike-slip fault that evolved into a normal fault with downthrow of its eastern side (Genna 1990).

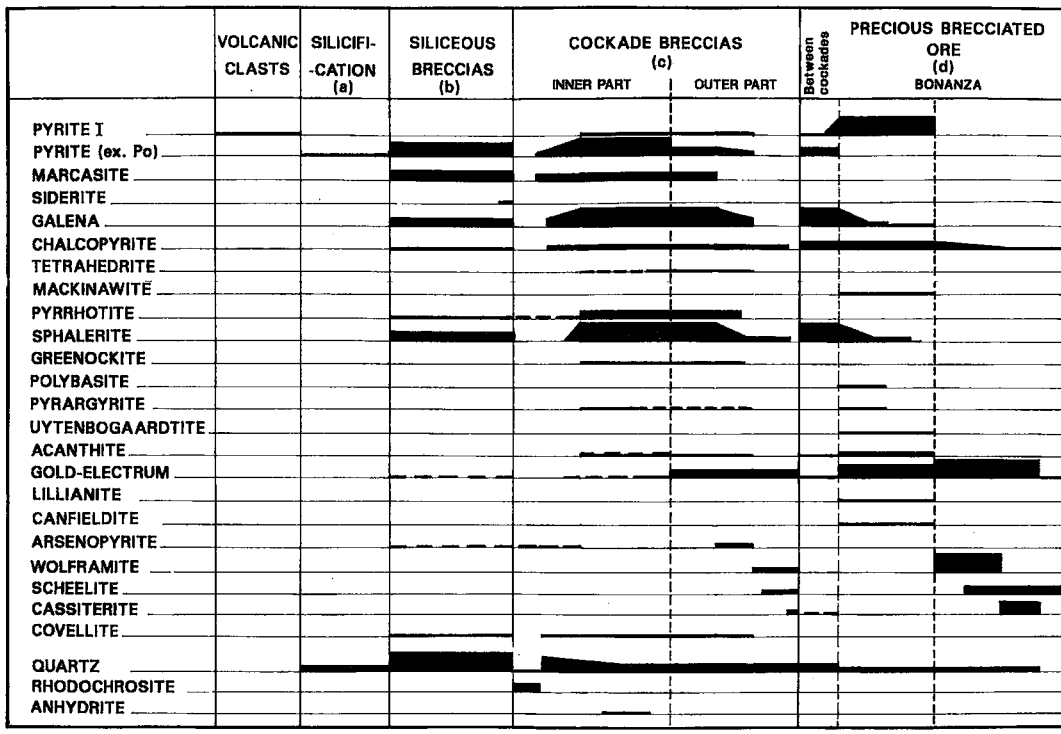


FIG. 2. Mineralogical succession of the Cirotan ore deposit.

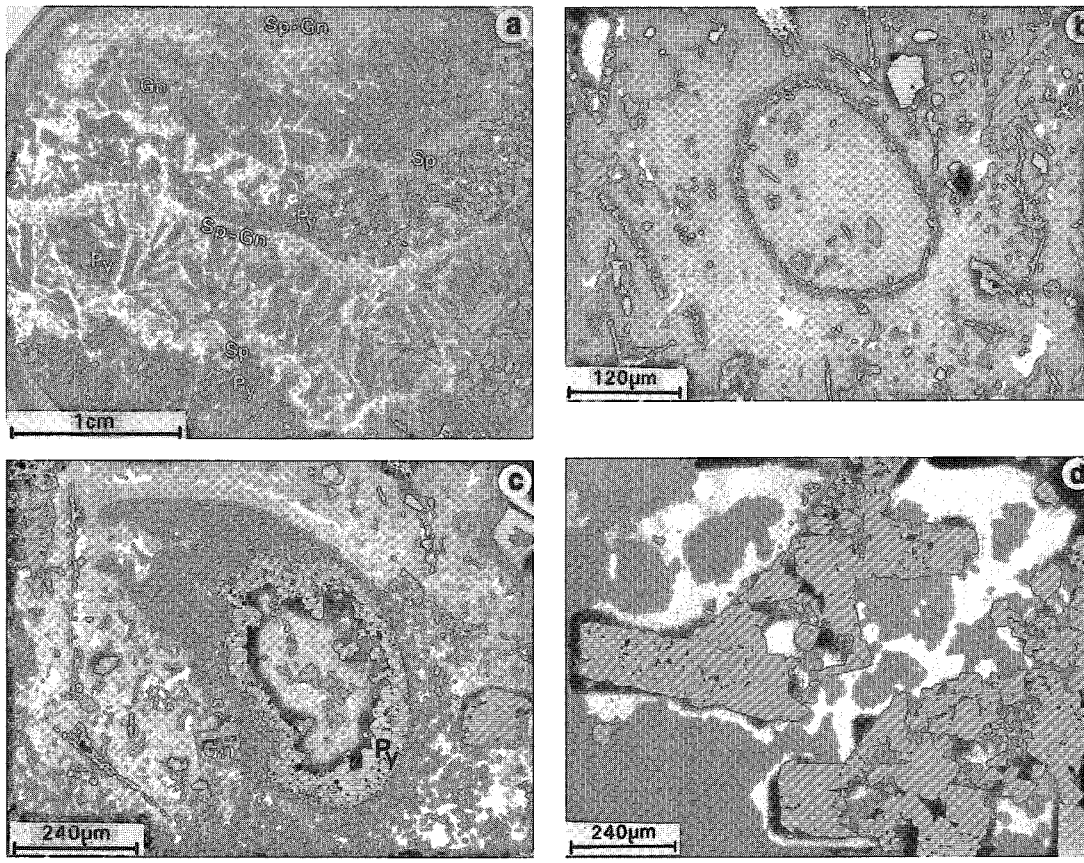


FIG. 3. a. Cockade breccias: banded texture of the sulfide envelopes. Most of the pyrite is pseudomorphic after pyrrhotite. CI 50, level L1000, SP49982. b. Bonanzas: bacillary pyrite (white) (with sphalerite), sphalerite "atoll" (grey), and disseminated pyrite in quartz (black). Level L1000, SP48645. c. Bonanzas: sphalerite (grey) + galena "oolith" partially infilled with pyrite, and bacillary pyrite. Level L1000, SP48645. d. Cockade breccias: pyrite pseudomorphs after pyrrhotite (white) invaded by sphalerite (grey) and galena (pale grey) in a quartz gangue (black). Note the volume loss caused by the pyrrhotite–pyrite transformation. Level L1000, CI46, SP49978. Symbols: Gn galena, Py pyrite, Sp sphalerite. Photos taken in reflected light.

## TYPES OF ORE

The mineralized structure at Cirotan contains four facies of ore (Milési *et al.*, in press), each associated with a stage in the evolution and increasing complexity of the structure (Fig. 2): (a) Intensive silicification of the country rocks over a width of 20–30 m, mainly in the footwall of the structure. (b) Siliceous breccias, between 0.1 and 22.5 m thick, comprising a matrix of banded chalcedonic quartz incorporating angular fragments of volcanic rock, quartz or sulfides, and evolving toward a poorly developed cockade facies. In places, these breccias pass to banded sulfide ore with vugs encrusted by spheroidal siderite. This facies has low grades of gold (<1.5 g/t Au) and is not mined, apart from rare sulfide pockets, where the gold grade can reach 2 g/t. (c) Cockade breccias, formed of clasts surrounded by rhodochrosite and then by envelopes of sulfides (Fig. 2). They differ from the siliceous breccias (b) in their degree of development (better-marked cockades, richer in sulfides), and in containing ovoid fragmented clasts showing clear rotation and friction movements. The sulfide envelopes (with cumulative thicknesses commonly of 0.10 m, and in places 0.40 m) are concentric around rounded or angular, variably sized (0.03–0.60 m, but in places as much as 1.0 m) volcanic, quartz or sulfide fragments. They show a rhythmic deposition (Fig. 3a) of a nearly identical sequence of minerals, with (1) pyrite, (2) galena ± chalcopyrite, and (3) sphalerite as the major minerals. The cockade breccias occur below level L800, mainly at the hanging-wall of the siliceous breccias (b), and are generally thinner than the siliceous breccias (15 m at level L900). These breccias are slightly auriferous but only rarely mined (2.0 to 2.5 g/t Au). (d) Precious brecciated ore, which occurs

as two subfacies: (1) "between cockade" ore of limited extent, occupying the empty spaces between cockades, and (2) "bonanza" ore, filling the spaces between breccia bodies. The bonanzas form lenticular bodies (0.2–3.5 m thick) intercalated within and containing fragments of the breccias (b) and (c). They do not show a rhythmic deposition of sulfides like the cockade breccias, but have a brecciated, cataclastic texture that is locally banded and is related to the strike-slip movement. This ore facies is the richest in gold (on average, 9–12 g/t Au with peaks of 700 g/t Au). (e) A late barren vuggy quartz encrusts vugs in all the mineralized facies.

Cirotan also shows original textures such as "bacillary" pyrite (up to 0.8 mm long) that is fairly commonly disseminated in the quartz. It originates from the transformation of pyrrhotite and forms partial infill "atoll" or "oolitic" textures (as much as 1.5 mm long) with sphalerite walls (Figs. 3b, c). The significance of these textures, which are reminiscent of certain textures typical of submarine mineralization (Fouquet *et al.* 1988), is not clear. The "atolls" could correspond to microfeeder channels in a fluid-supersaturated environment.

Facies (a) is pyritic only, and facies (b) is very poor in sulfides; pyrite and lamellar marcasite (pseudomorphs after pyrrhotite), sphalerite, galena and rare chalcopyrite and arsenopyrite are present, and gold is very rare. Facies (c) and (d), on the other hand, are very rich in sulfides (Fig. 2); the gangue is predominantly quartz–sericite with, in the cockade breccias, abundant rhodochrosite (± rhodonite) below level L800, in places associated in vugs with acicular parsettensite [$Mn_5Si_6O_{13}(OH)_8$]; orthoclase (adularia habit) and apatite are fairly common as small euhedral crystals (100–150 μm) disseminated in quartz crystals;

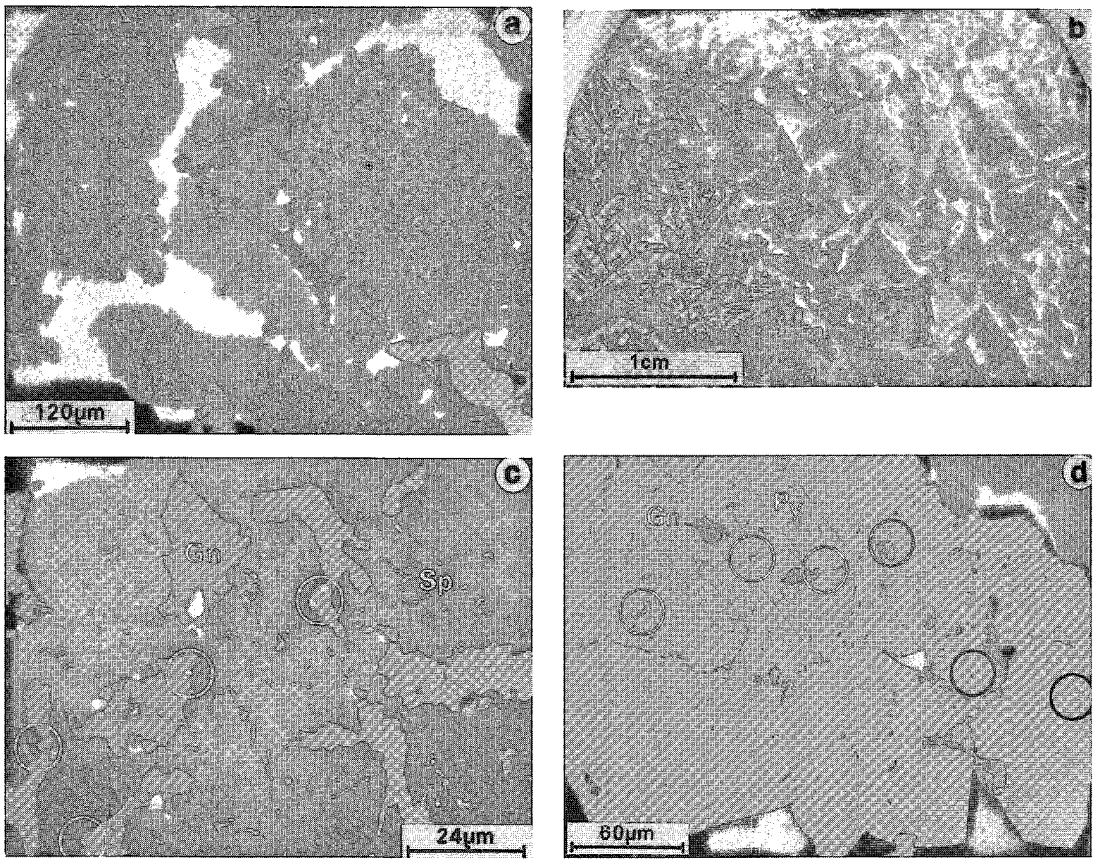


FIG. 4. a. Cockade breccias: graphic texture of galena + chalcopyrite association (white) in sphalerite (grey). Level L1000, CI43, SP49974. b. Cockade breccias: skeletal texture of galena (white) + sphalerite (white) association. Level L1000, CN21, SP51044. c. Cockade breccias: electrum (circles) in galena in contact with sphalerite rich in chalcopyrite microinclusions. Level L1000, CI46, SP49979. d. Cockade breccias: electrum (circles) in pyrite, commonly in contact with galena inclusions. Level L1000, CI56, SP49983. Symbols as in Fig. 3. Photos taken in reflected light.

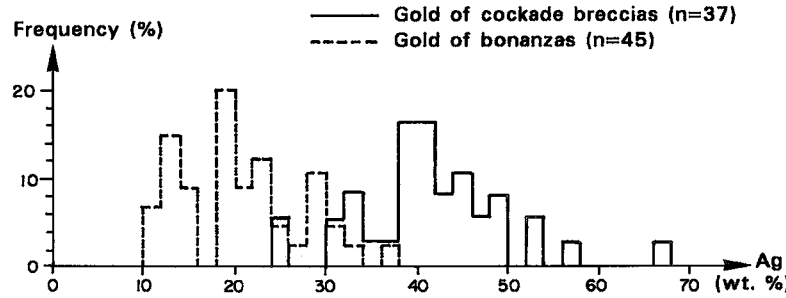


FIG. 5. Silver contents of electrum in the cockade breccias and bonanzas. Results of electron-microprobe analyses (BRGM, CAMECA SX 50). Analytical conditions: acceleration voltage 20 kV, current intensity 20 nA; standards: pure Ag (Ag$L\alpha$) and pure Au (Au$L\alpha$).

gypsum and anhydrite (200 to 400 μm) are rare, as is calcite; no fluorine-bearing mineral (such as topaz) nor tourmaline has been observed.

## MINERALOGY OF THE COCKADE BRECCIAS

### *Common minerals*

The cockade breccias are formed of dominant bands of quartz – pyrrhotite – galena – sphalerite in which the pyrrhotite was transformed to pyrite during the deposition of galena + sphalerite, and of thin bands of quartz – pyrite – galena – sphalerite.

Pyrite, the dominant sulfide in the cockade envelopes, forms polycrystalline masses associated with marcasite and shows all the characteristics of being a complete pseudomorph of pyrrhotite (Picot & Johan 1983, Murowchick 1992): the squat shape of pyrrhotite prisms is preserved, and about 20–30 modal % pore space is filled with byproducts (mainly magnetite) or manifested by a cavity at the center of the pseudomorph (Fig. 3d). The pyrite bands consist of rows of prismatic crystals, 1–10 mm long, showing an alignment perpendicular to the banding in the first rows and then arranged haphazardly in the later rows. Primary euhedral crystals of pyrite are rare, small, and commonly associated with the thinner bands containing dominant sphalerite.

Sphalerite and galena are common in the concentric envelopes and form generally thin (1–20 mm), regular and continuous bands. The relationships between the two sulfides are complex and give rise to noteworthy textures (*e.g.*, arborescent and graphic, very similar to those of graphic pegmatite: Fig. 4a) that suggest rapid and partly synchronous crystallization in a medium that was fluid-saturated or under high fluid pressure. Nevertheless, a study of the samples and the numerous cases of replacement-corrosion of galena by sphalerite (skeletal textures, Fig. 4b), with inclusions of greenockite, show that the deposition of galena in part preceded that of the sphalerite within a single sequence.

Chalcopyrite is common, but much less abundant than the preceding sulfides. It occurs as fairly large irregular patches (up to 1 mm) in the galena, and as myriads of inclusions of variable size (0.1–200 μm) commonly forming swarms within the sphalerite. Other minerals are less common. Pyrrhotite, after having precipitated in abundance at the beginning of each depositional sequence, was totally replaced by pyrite. It remains only as inclusions within sphalerite, associated with small patches of galena, chalcopyrite and, in places, gold. Pyrargyrite ($Ag_3SbS_3$) forms rare small patches (10–20 μm) in the galena, in places associated with tetrahedrite ($Cu_{12}Sb_4S_{13}$) at the edges of patches of chalcopyrite, and with acanthite ($Ag_2S$; optical determinations confirmed by SEM analysis).

Electrum is a common mineral in the cockade breccias. It is silver-rich (24–68 wt.% Ag, with an average value around 40 wt.% Ag), grading in places into native silver (Fig. 5), which occurs mainly in millimeter-thick bands with the sphalerite and primary pyrite that close the mineral sequences. In the sphalerite (67% of the observed patches), electrum appears

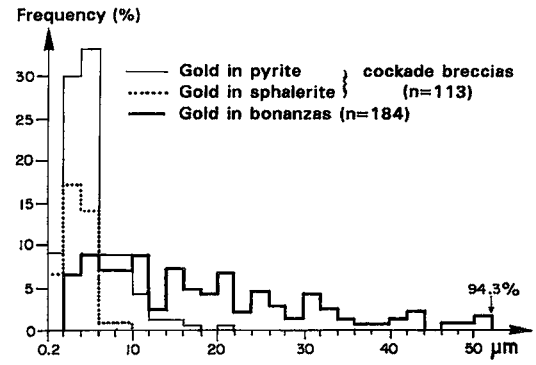


FIG. 6. Comparative sizes of electrum patches in the cockade breccias and bonanzas.

TABLE 1. COMPOSITION OF Zn-BEARING GREENOCKITE FROM CIROTAN

| | 1 | 2 | 3 | 4 | 5 | 6 | 7 | 8 | 9 | 10 | Mean | at.% |
|---|---|---|---|---|---|---|---|---|---|---|---|---|
| Zn | 3.78 | 6.10 | 3.71 | 5.31 | 5.92 | 6.33 | 4.79 | 6.27 | 4.79 | 6.80 | 5.4 | 5.77 |
| S | 21.69 | 22.15 | 21.78 | 21.93 | 21.94 | 22.65 | 22.33 | 22.39 | 21.99 | 22.74 | 22.1 | 48.51 |
| Cd | 74.76 | 71.60 | 75.52 | 73.78 | 72.71 | 71.78 | 73.63 | 73.48 | 73.68 | 70.98 | 73.2 | 45.72 |
| Σ | 100.24 | 99.85 | 101.02 | 101.02 | 100.57 | 100.77 | 100.76 | 102.15 | 100.48 | 100.53 | 100.7 | |
| | 11 | 12 | 13 | 14 | 15 | 16 | 17 | 18 | 19 | 20 | Mean | at.% |
| Zn | 5.43 | 6.37 | 6.48 | 3.58 | 3.20 | 4.58 | 2.47 | 2.54 | 4.03 | 2.21 | 4.1 | 4.49 |
| S | 22.01 | 22.22 | 22.06 | 21.65 | 21.95 | 21.96 | 21.79 | 21.40 | 21.83 | 21.33 | 21.8 | 48.97 |
| Cd | 71.88 | 69.59 | 70.16 | 73.17 | 74.07 | 71.81 | 73.90 | 74.65 | 72.33 | 75.13 | 72.7 | 46.53 |
| Σ | 99.33 | 98.19 | 98.71 | 98.41 | 99.23 | 98.36 | 98.18 | 98.60 | 98.19 | 98.67 | 98.6 | |

**Results of electron-microprobe analyses (BRGM, CAMECA SX 50) are quoted in wt.%. Analytical conditions: acceleration voltage 20 kV, current intensity 20 nA; standards: compounds ZnS (ZnKα, SKα), pure Fe (FeKα), pure Cd (CdLα). The iron content is less than 1 wt.%.**

as very small patches (0.5–8.0 μm) in contact with the galena, chalcopyrite or pyrrhotite inclusions (Fig. 4c), whereas in the primary pyrite (Fig. 4d), the patches are larger (5–20 μm; Fig. 6). Much more rarely, electrum forms small spots in the galena. It has not been observed in the pyrite derived from the transformation of pyrrhotite.

*Uncommon minerals*

In addition to the above common minerals, the cockade breccias are distinguished by more exceptional minerals for this type of deposit, such as Zn-bearing greenockite in 200–300 μm patches included in the sphalerite of the cockades. Contrary to the general rule (Picot & Johan 1983), it does not show the internal lemon-yellow reflections characteristic of this mineral. Electron-microprobe analyses reveal the constant presence of Zn, with an average of 4.1 wt.% (Table 1).

The outermost envelopes of the cockades lying close to or in contact with terminal quartz vugs show a dissemination of arsenopyrite, ferberite–scheelite, and rare cassiterite in the sulfides. The arsenopyrite forms small euhedral to subhedral crystals isolated in the quartz or encrusting the pyrite; it shows no particular zonation, and As contents vary randomly between 29.0 and 33.8 at.%, in places within a single crystal. Acicular crystals (length/width in the range 10–20) of ferberite [$(Fe,Mn)WO_4$] are fairly uncommon and small (20–240 μm); they show an impressive compositional variation (64–90 mole % $FeWO_4$; Fig. 7) and are everywhere variably replaced by scheelite ($CaWO_4$). Rare crystals of cassiterite have nucleated on the wolframite crystals.

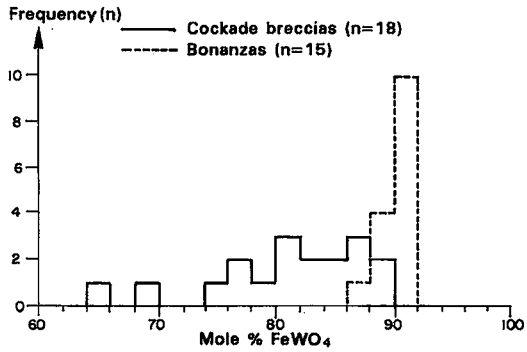


FIG. 7. Mole % $FeWO_4$ of ferberite in the cockade breccias and bonanzas. Results of electron-microprobe analyses (BRGM, CAMECA SX 50). Conditions of analysis: see Table 6.

## MINERALOGY OF THE PRECIOUS BRECCIATED ORE

*Common minerals*

The "between cockade" ore is formed mainly of sphalerite + galena (showing the same noteworthy textures as in the cockade breccias), with minor pyrite, marcasite, chalcopyrite, acanthite, electrum and rare cassiterite.

The exceptionally rich ore shoots, here called "bonanzas", possess a more complex paragenesis

(Fig. 2). Apart from pyrrhotite and tetrahedrite, which have not been observed, they contain most of the minerals of the cockade breccias. Pyrite is very abundant and, unlike that of the cockade breccias, is totally primary, with a poikiloblastic texture unknown in the cockade breccia ores. Galena and sphalerite are less common, whereas chalcopyrite, rich in mackinawite [$(Fe,Ni)_9S_8$] inclusions, is more developed. The silver minerals are diversified and increase in proportion; polybasite ($Ag_{16}Sb_2S_{11}$) appears within the galena at the edges of the pyrargyrite; acanthite is locally abundant, especially in the zone of recent cementation (level L500), where it is associated with covellite and with galena, or it occurs at the edges of patches of pyrite, in places accompanied by electrum.

*Uncommon minerals*

The major original feature of the precious brecciated ore is the development of a late W – Sn – Au – Ag – (Te–Bi) sequence that progressively replaces the base-metal paragenesis. This late assemblage occurs mainly disseminated in the sulfides of the bonanzas, but may also occur within a fine network of quartz (<5 mm in thickness) cutting the sulfides. These "super-bonanzas", easily recognized by the needles of wolframite, form the richest parts of the deposit (400 g/t Au, 5.5% W, and 2.7% Sn).

Uytenbogaardtite ($Ag_3AuS_2$) appears as small patches (50 μm) within the pyrite, systematically associated with electrum (74.6 wt.% Ag), acanthite or Te-

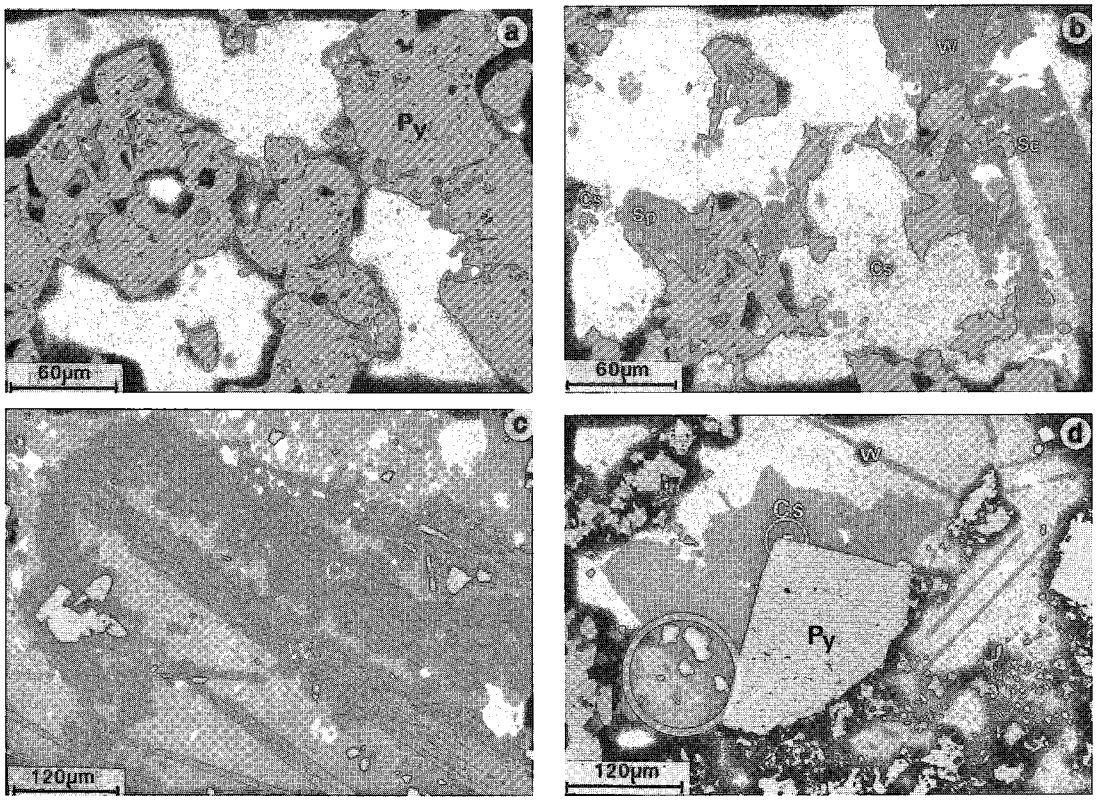


FIG. 8. a. Bonanzas: patches of canfieldite, and in places uytenbogaardtite (grey, not distinguishable on the photo) in pyrite. Level 1000, CN22, SP51045. b. Bonanzas: Lillianite (pale grey) associated with electrum (white), sphalerite and wolframite, partially transformed to scheelite. Cassiterite also is disseminated in the quartz. Level L1000, CN22, SP51287. c. Bonanzas: Large acicular crystals of wolframite encrusted by cassiterite in quartz. Pyrite (white) deposited at the beginning of the bonanza stage also is covered by cassiterite. Open pit, CR72, SP51640. d. Bonanzas: Euhedral cassiterite deposited on a fragment of pyrite. Note the breccia appearance due to fragments of pyrite (white) and wolframite disseminated in the quartz. Patches of gold (circles) accompany the cassiterite. Level 1000, CN22, SP51708. Symbols: Cs cassiterite, W wolframite, Sc scheelite; others as in Fig. 3. Photos taken in reflected light.

TABLE 2. COMPOSITION OF UYTENBOGAARDTITE FROM CIROTAN

| | | | | Mean | at.% | at.=6 |
|---|---|---|---|---|---|---|
| S | 10.22 | 11.02 | 11.84 | 11.0 | 33.9 | 2.04 |
| Se | 0.03 | 0.04 | 0.04 | - | - | - |
| Ag | 48.59 | 51.04 | 52.08 | 50.6 | 46.4 | 2.74 |
| Te | 0.08 | 0.18 | 0.09 | 0.1 | - | - |
| Au | 40.63 | 38.99 | 38.35 | 39.3 | 19.7 | 1.16 |
| Σ | 99.55 | 101.27 | 102.40 | 101.0 | | |

Results of electron-microprobe analyses (BRGM, CAMECA SX 50), expressed in wt.%. Analytical conditions: see Table 1. Standards: FeS (SKα), pure Ag (AgLα), pure Au (AuLα), pure Se (SeLα), pure Te (TeLα).

bearing canfieldite (Fig. 8a). Optical determinations of these minerals have been confirmed by SEM and electron-microprobe analyses. The structural formula of uytenbogaardtite, calculated from results of electron-microprobe analyses (Table 2), is $Ag_{2.3}AuS_{1.7}$, with Ag/Au (atom) and (Ag+Au)/S (atom) ratios of 2.3 and 1.94, respectively. These figures are slightly different from those for the uytenbogaardtite defined by Barton *et al.* (1978), $Ag_3AuS_2$, 3, and 2, respectively and could be related to the possible presence of fine exsolution-lamellae of acanthite.

Te-bearing canfieldite [$Ag_8Sn(S_{6-x}Te_x)$, where $x$ = 2] occurs as small ameboid patches (45 μm) within the pyrite (Table 3, Fig. 8a). It is in places associated, with acanthite or uytenbogaardtite and is the only telluride mineral at Cirotan. Unlike canfieldite *sensu stricto* ($Ag_8SnS_6$), its tendency to tarnish upon exposure is very limited. This rare mineral, first described by Harris & Owens (1971) in the pyrite – sphalerite – galena – cassiterite – scheelite deposit at Revelstoke, British Columbia, has since been reported in four other granite-related deposits: three are complex Bi – Mo – Sn – W – Pb – Te skarns from Japan (Soeda *et al.* 1984), and the fourth is the large W–Sn ore deposit of Panasqueira, Portugal (Wimmers 1985). The Te-bearing canfieldite at Cirotan is chemically closer to that of the Japanese skarns (18.5–20.3 wt.% Te) than to that of Revelstoke (13.9 wt.% Te) or Panasqueira (with Cu and Fe); it confirms the replacement of S by Te. In all its known occurrences, the Te-bearing canfieldite forms part of an assemblage characteristic of a relatively low state of oxidation and an intermediate degree of sulfidation and acidity (Soeda *et al.* 1984).

A complex Ag-, Pb-, Bi-bearing sulfosalt occurs as commonly agglomerated elongate fibers (200 μm) filling the quartz interstices (Fig. 9). It is almost everywhere associated with large patches of electrum and with wolframite, and seems to be contemporaneous with these minerals (Fig. 8b). Electron-microprobe analyses have revealed a very homogeneous composition having the simplified formula $AgPb_4Bi_5S_{12}$ (Table 4). The powder pattern confirms that this mineral belongs to the gustavite ($AgPbBi_3S_6$) – lillianite ($Pb_3Bi_2S_6$) homeotypic series, in which it forms a middle member (Table 5). This compound, corresponding to $Gus_{50}$ in the system of Makovicky & Karup-Møller (1977), is the richest member of the lillianite species in terms of Ag and Bi. According to these authors, a miscibility gap exists in the gustavite–lillianite homeotypic series between $Gus_{50}$ and $Gus_{85}$, whereas a chemical continuity exists between $Gus_{50}$ (AgBi-rich lillianite) and $Gus_0$ (pure lillianite). A very similar AgBi-rich lillianite ($Gus_{53}$) has been described at La Roche-Balue in France in association with gustavite (Gus ≥ 80) (Moëlo *et al.* 1987). The powder patterns of pure lillianite and gustavite, which are very similar, become indistinguishable with that for a AgBi-rich lillianite in a small-diameter camera (Table 5); they no longer constitute a discriminant criterion for identification. Lillianite is the only bismuth mineral observed at Cirotan. The rare minerals of the lillianite–gustavite

TABLE 3. COMPOSITION OF Te-BEARING CANFIELDITE FROM CIROTAN

| | | | | | | | | Mean | at.% | | (1) |
|---|---|---|---|---|---|---|---|---|---|---|---|
| S | 9.14 | 9.32 | 9.17 | 9.10 | 9.22 | 9.05 | 9.37 | 9.2 | 26.1 | 4 | 13.95 |
| Se | 0.13 | 0.30 | 0.20 | 0.30 | 0.23 | 0.22 | 0.31 | 0.2 | 0.2 | | |
| Ag | 63.90 | 63.60 | 64.47 | 64.36 | 63.55 | 64.85 | 63.50 | 64.0 | 54.2 | 8.24 | 65.12 |
| Sn | 8.53 | 8.12 | 8.32 | 8.96 | 8.25 | 8.00 | 8.13 | 8.3 | 6.4 | 0.97 | 8.69 |
| Te | 18.43 | 17.81 | 18.25 | 17.99 | 18.35 | 18.40 | 18.34 | 18.2 | 13.0 | 1.98 | 13.95 |
| Σ | 100.13 | 99.15 | 100.41 | 100.71 | 99.60 | 100.52 | 99.65 | 99.9 | 98.33 | | |

Results of electron-microprobe analyses (BRGM, CAMECA SX 50), in wt.%. Analytical conditions: see Table 1. Standards: pure Sn (SnLα), pure Te (TeLα), pure Ag (AgLα), pure Se (SeLα), FeS (SKα). (1): Te-bearing canfieldite from Revelstoke, B.C. (Harris & Owens 1971).

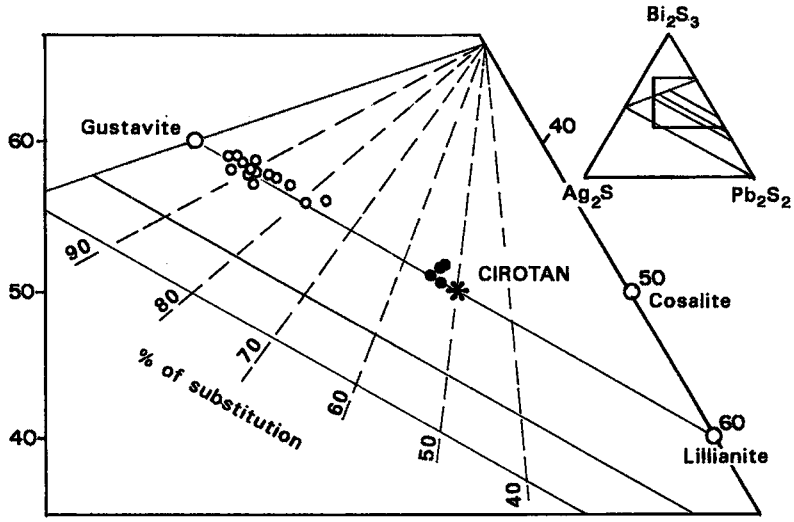


FIG. 9. Projection of lillianite compositions from Cirotan in the $Pb_2S_2$–$Bi_2S_3$–$Ag_2S$ system. Data on the gustavite (•) and the lillianite (○) of La Roche-Balue are from Moëlo *et al.* (1987).

series appear in acidic magmatic settings and seem to indicate the transition between the pneumatolytic and hydrothermal domains, *e.g.*, at La Roche-Balue, where they are associated with scheelite (Moëlo *et al.* 1987), at Tanco in Manitoba (Harris & Chen 1975), and in the tungsten district of Monteneme in Spain (Gouanvic & Babkine 1985).

In addition to these unusual minerals cogenetic with the pyrite, ferberite forms tufts of larger acicular crystals (as much as 8 mm long) partially transformed to scheelite and generally separated from the sulfides by a quartz rim (Fig. 8c). Results of electron-microprobe analyses of the ferberite show a very constant composition (88–92 mole % $FeWO_4$; Fig. 7).

Cassiterite occurs as millimeter-size areas of twinned euhedral crystals encrusting pyrite and ferberite–scheelite crystals (Figs. 8c, d). It contains (Table 6) iron (2.6–3.9 wt.% FeO), tantalum (0.2–0.4 wt.% $Ta_2O_5$) and indium (0.1–0.7 wt.% $In_2O_3$), but no Nb or Mn. No inclusion of magnetite or columbite–tantalite has been observed. The deposition of cassiterite continued after that of wolframite and chalcopyrite. Only scheelite, in patches several millimeters across, fills the late quartz vugs and appears after cassiterite (Fig. 10a); this scheelite is hypogene, and no longer formed at the expense of the ferberite.

Gold is more common in the precious brecciated ores than in the cockade breccias; it forms larger parti-

TABLE 4. COMPOSITION OF Ag-Bi-RICH LILLIANITE FROM CIROTAN

| | | | | | | | | | | | | Mean | at.% | (S+Se) = 12 |
|---|---|---|---|---|---|---|---|---|---|---|---|---|---|---|
| Ag | 5.11 | 4.89 | 4.75 | 4.94 | 4.83 | 4.79 | 4.96 | 4.68 | 4.72 | 4.47 | 5.08 | 4.84 | 4.89 | 1.08 |
| Bi | 44.10 | 42.86 | 44.87 | 45.07 | 42.13 | 43.71 | 43.71 | 44.24 | 44.71 | 42.26 | 43.04 | 43.70 | 22.79 | 5.03 |
| Pb | 33.47 | 34.56 | 32.93 | 32.83 | 36.88 | 33.64 | 34.66 | 33.24 | 33.77 | 36.32 | 34.30 | 34.23 | 18.01 | 3.98 |
| Se | 0.60 | 0.62 | 0.61 | 0.74 | 0.62 | 0.54 | 0.56 | 0.61 | 0.58 | 0.56 | 0.62 | 0.60 | 0.83 | 12 |
| S | 15.53 | 15.99 | 15.78 | 15.88 | 15.86 | 15.85 | 15.63 | 15.66 | 15.48 | 15.52 | 15.87 | 15.73 | 53.48 | |
| Σ | 98.96 | 98.93 | 98.94 | 99.50 | 100.49 | 98.89 | 99.58 | 98.47 | 99.60 | 99.37 | 99.05 | 99.10 | | |

Results of electron-microprobe analyses (BRGM, CAMECA SX 50), in wt.%. Analytical conditions: see Table 1. Standards: FeS (FeKα, SKα), PbS (PbMα), pure Ag (AgLα), pure Bi (BiMα), pure Se (SeLα).

TABLE 5. X-RAY POWDER DIAGRAM OF Ag-Bi-RICH LILLIANITE AND COMPARISON WITH SAMPLES OF GUSTAVITE AND SYNTHETIC LILLIANITE

| CIROTAN LILLIANITE | | CAMSELL RIVER GUSTAVITE | | IVIGTUT GUSTAVITE | | SYNTHETIC LILLIANITE | |
|---|---|---|---|---|---|---|---|
| d(Å) | I | d(Å) | I | d(Å) | I | d(Å) | I |
| 3.998 | 3 | 3.973 | 4 | 3.977 | 5 | | |
| 3.646 | 6 | 3.667 | 4 | 3.640 | 8 | 3.52 | 10 |
| | | | | 3.401 | 8 | 3.42 | 7 |
| 3.381 | 10 | 3.379 | 10 | 3.376 | 8 | | |
| | | | | 3.363 | 10 | | |
| 2.997 | 6 | 3.007 | 6 | 2.998 | 10 | 3.01 | 6 |
| 2.897 | 7 | 2.900 | 8 | 2.895 | 10 | 2.91 | 8 |
| 2.748 | 4 | 2.759 | 4 | | | 2.78 | 6 |
| 2.286 | 2 | 2.287 | 3 | | | | |
| - | | 2.260 | 3 | | | | |
| 2.131 | 3 | 2.131 | 4 | | | | |
| 2.089 | 2 | 2.070 | 4 | | | 2.07 | 6 |
| 2.049 | 6 | 2.048 | 8 | | | | |
| 1.959 | 2 | 1.959 | 5 | | | | |
| - | | 1.907 | 4 | | | | |
| 1.755 | 4 | 1.755 | 5 | | | 1.78 | 7 |

Comparison is made with the X-ray powder diagram of gustavite from Ivigtut, Greenland (Karup-Møller 1970), which is composed of a gustavite-lillianite intergrowth, and from Camsell River, British Columbia (Harris & Chen 1975), as well as with synthetic lillianite (Anthony et al. 1990). Analyst: F. Pillard, SGN/GEO, BRGM; CuKα radiation, Debye-Scherrer camera, 76.4 mm in diameter). The intensity of the peaks is estimated.

cles of different habit (Fig. 6), and its silver content is lower (10–38 wt.% Ag, with an average value around 18–20 wt.% Ag; Fig. 5). It occurs as large patches (as much as 60 μm) in the pyrite, alone or associated with uytenbogaardtite (Fig. 10b). Most of the gold, however, is associated with ferberite–cassiterite, where it occurs as patches of 4 to 230 μm (average 16–50 μm) deposited on the wolframite within areas of cassiterite (Figs. 10c, d) or isolated in the quartz gangue. Electrum and scheelite were last to be deposited in the episode of mineralization at Cirotan.

## Conditions of Deposition

An extensive microthermometric study of quartz- and sphalerite-hosted fluid inclusions was performed on samples from the different stages of mineralization (Nehlig & Marcoux 1992). The main results are presented here in order to consider the other physicochemical parameters in relation to the findings. The fluid inclusions are large (10–100 μm), aqueous and two-phase: liquid + vapor. They comprise pseudosecondary inclusions trapped in the sphalerite, and primary, pseudosecondary, and secondary inclusions in the quartz (classification of Roedder 1984).

The temperatures of homogenization of the fluid inclusions in sphalerite are tightly clustered (207 to 280°C, with sample averages between 232 and 255°C). The temperatures of homogenization of the inclusions in quartz (except for the final vuggy quartz) are generally similar to those from sphalerite (averages between 245 and 256°C). The temperatures show an overall increase from the cockade breccias (c) to the bonanzas (d), and only fall with the deposition of the final vuggy quartz (e). It can thus be considered that the whole of the gold mineralization was deposited at about 245 ± 40°C, which is similar to the temperatures of deposition determined for other epithermal adularia–sericite deposits (Hayba *et al.* 1985, Heald *et al.* 1987). The salinities of the inclusions from both sphalerite and quartz also show an increase, from 2.89 to 7.15 wt.% eq. NaCl, during the depositional stages of the mineralization. The highest values are found in the bonanza stage (d) (5.09 to 7.15 wt.% eq. NaCl) and the terminal vuggy quartz stage (e) (4.01 to 5.85 wt.% eq. NaCl). The transition from the cockade breccias to the precious brecciated ore is thus marked by a noticeable increase in the salinity of the fluids.

### *Conditions of deposition of the cockade breccias*

The iron content of the sphalerite in the cockade breccias varies between 0.5 and 26 mole % FeS (Fig. 11). The high contents (19–26 mole % FeS) are restricted to sphalerite with numerous inclusions of pyrrhotite at the beginning of each sequence, and the

TABLE 6. COMPOSITION OF CASSITERITE FROM CIROTAN

| | | | | | | | | | | | | | | | | | Mean |
|---|---|---|---|---|---|---|---|---|---|---|---|---|---|---|---|---|---|
| $SnO_2$ | 94.73 | 95.37 | 94.80 | 96.43 | 94.00 | 95.32 | 95.21 | 96.41 | 95.28 | 95.56 | 94.44 | 93.29 | 94.20 | 95.45 | 94.03 | 93.95 | 94.90 |
| $Nb_2O_5$ | 0.13 | 0.11 | - | - | 0.08 | - | - | - | 0.07 | 0.04 | - | - | - | - | - | - | - |
| FeO | 3.28 | 3.12 | 3.23 | 3.21 | 3.40 | 3.04 | 3.35 | 2.95 | 3.33 | 3.48 | 3.59 | 3.13 | 3.07 | 2.86 | 3.88 | 2.59 | 3.22 |
| $Ta_2O_5$ | 0.32 | 0.39 | 0.37 | 0.32 | 0.28 | 0.39 | 0.29 | 0.28 | 0.38 | 0.38 | 0.34 | 0.40 | 0.32 | 0.22 | 0.39 | 0.47 | 0.34 |
| $In_2O_3$ | 0.50 | 0.33 | 0.48 | 0.43 | 0.54 | 0.54 | 0.28 | 0.42 | 0.11 | 0.20 | 0.32 | 0.41 | 0.74 | 0.12 | 0.05 | 0.52 | 0.37 |
| MnO | - | 0.03 | - | 0.05 | - | 0.02 | 0.06 | - | - | - | - | - | 0.02 | 0.10 | - | - | - |
| Σ | 98.96 | 99.35 | 98.89 | 100.44 | 98.30 | 99.31 | 99.19 | 100.06 | 99.17 | 99.66 | 98.70 | 97.23 | 98.35 | 98.75 | 98.35 | 97.54 | 98.83 |

Results of electron-microprobe analyses (BRGM, CAMECA SX50), in wt. %. Analytical conditions: see Table 1. Standards: FeS (FeKα), pure Ta (TaMα), $MnTiO_3$ (MnKα), pure Nb (NbLα), pure In (InMα), SnO (SnLα), pure W (WMα).

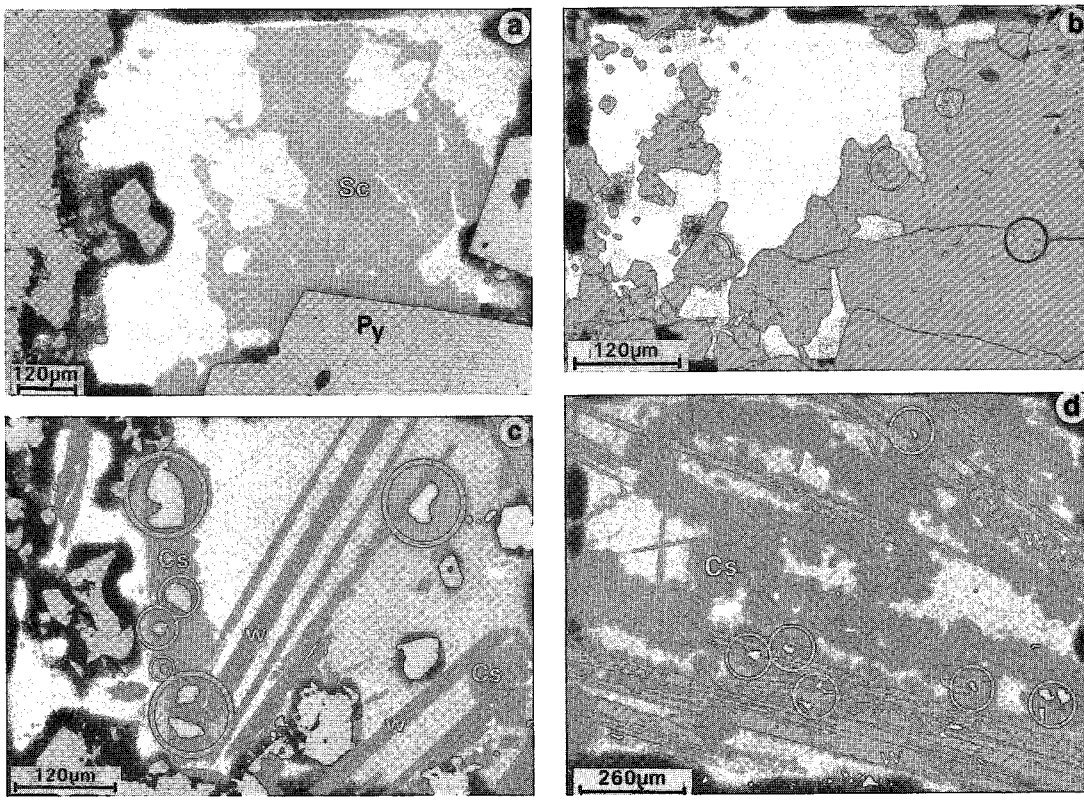


FIG. 10. a. Bonanzas: Terminal quartz vug filled with scheelite. Level L1000, CN22, SP51708. b. Bonanzas: electrum (circles) in primary pyrite. Level L1000, CN22, SP51286. c. Bonanzas: electrum (circles) associated with cassiterite and wolframite. Note the cassiterite deposit on the wolframite as well as the breccia texture of the mineralization due mainly to fragmentation and corrosion of the pyrite. Level L1000, CN22, SP51707. d. Bonanzas: Association of electrum (circles), cassiterite and wolframite, from the very rich part of the deposit. Open pit, CR72, SP51640. Symbols as in Figs. 3, 4 and 8. Photos taken in reflected light.

lowest contents (< 5 mole % FeS) are associated with the rare primary pyrite and the ferberite–scheelite of the outer envelopes of the cockades, marking the end of this stage. Thus the deposition of a mineralized sequence appears to have begun in the stability field of pyrrhotite [*i.e.*, $f(S_2)$ close to $10^{-13}$ at 250°C and close to $10^{-12}$ atm if deposition began at 290°C) and continued in the pyrite field. The crossing of the pyrrhotite–pyrite join during a drop in temperature, probably associated with an increase in $f(S_2)$, enabled re-equilibration of almost all the pyrrhotite. If deposition of the sequence was completed around 200°C, $f(S_2)$ could only reach $10^{-9}$, since the increase in $f(S_2)$ would be limited by the absence of the association bornite + pyrite (Fig. 12). This is consistent with the results of Murowchick (1992), who showed that a solution formed by dissolution of pyrrhotite can easily give rise to one that is extremely supersaturated with respect to pyrite.

The presence of cogenetic pyrite and marcasite after pyrrhotite could indicate a pH of about 5 (Murowchick 1992) for the transformation. Variations in the arsenopyrite composition (29.0 to 33.8 at.% As) could also reflect variations in $f(S_2)$ during deposition. The gold is associated indifferently with both types of sphalerite. The Zn-bearing greenockite, on the other hand, occurs with sphalerite with 5–15 mole % FeS, *i.e.*, exclusively in the stability field of pyrite.

The end of the cockade breccia stage (c) was marked by the synchronous deposition of wolframite–sphalerite, denoting lower $f(S_2)$ conditions, which could have resulted from a drop in $f(S_2)$ at constant $f(O_2)$ ($\sim 10^{-35}$) atm caused by the precipitation of sulfides. The sphalerite is iron-poor (< 5 mole % FeS), but Cd-rich (as much as 2.2 wt.% Cd), and is in every way similar to that of the bonanzas (Fig. 11). The oxidizing conditions that briefly occurred at the end of the deposition of the cockade breccia were thus a precursor to a more oxidizing geochemical climate that developed during the bonanza stage.

*Conditions of deposition of the bonanzas*

The bonanzas were formed at similar temperatures as the cockade breccias, but with different mineralogical assemblages, firstly, sulfide-rich with quartz – pyrite – (galena) – sphalerite – (gold), then oxide-rich, with quartz – wolframite – cassiterite – (gold, chalcopyrite) – scheelite. A significant difference with respect to the cockade breccias is the absence of pyrrhotite.

The primary pyrite is associated with iron-poor sphalerite (2–5 mole % FeS) that is rich in Cd (as much as 1.4 wt.% Cd), a factor that coincides with the disappearance of greenockite (Fig. 11). The beginning of deposition therefore took place with an average $f(S_2)$ around $10^{-12}$ to $10^{-11}$ atm (at 250°C), the absence of stannite–stannoidite imposing a maximum $f(S_2)$ of $10^{-9}$ atm at this temperature (Shimizu & Shikazono 1987). Such conditions inhibit the formation of greenockite, but allow the appearance of uytenbogaardtite, acanthite, electrum and Te-bearing canfieldite, the textures suggesting synchronous deposition with quartz – galena – sphalerite – pyrite. The genesis of the uytenbogaardtite is not clearly established, and could merely indicate a disequilibrium of the pair argentite–electrum during cooling of the system, since this mineral is only stable below 185°C (Barton *et al.* 1978).

The presence of Te-bearing canfieldite suggests an acidic environment, with a low fugacity of oxygen and an intermediate degree of sulfidation (Soeda *et al.* 1984), which could represent a transition with the depositional phase of ferberite and cassiterite. The temperature conditions for the formation of this mineral are poorly known (Soeda *et al.* 1984), but could be of the order of 275°C at Panasqueira (Wimmers 1985), which is consistent with the temperature of about 250°C estimated at Cirotan from the fluid inclusions.

The later appearance of ferberite, and then cassiterite–scheelite, implies a shift to lower $f(S_2)$ conditions, outside the pyrite – pyrrhotite stability field (Fig. 13). Such conditions could, as in the cockade breccias, result from the exhaustion of available sulfur, causing a drop in the $f(S_2)$ and a shift of the equilibrium to the oxide field. The rare cogenetic sulfides (sphalerite, and then only chalcopyrite) are those that possess a wide field of stability. At 250°C (temperatures obtained from the fluid inclusions), ferberite only is stable up to a maximum $f(O_2)$ of $10^{-14}$ atm (Hsu 1976). The evolution of the ferberite compositions (from 64–90 mole % $FeWO_4$ in the cockade breccias to 88–92 mole % $FeWO_4$ in the bonanzas) may be due to a decreasing Mn/Fe ratio in the mineralizing solution with time, as at the San Cristobal deposit in Peru (Campbell & Petersen 1988). The use of the Mn/Fe ratio for geothermometric purposes is

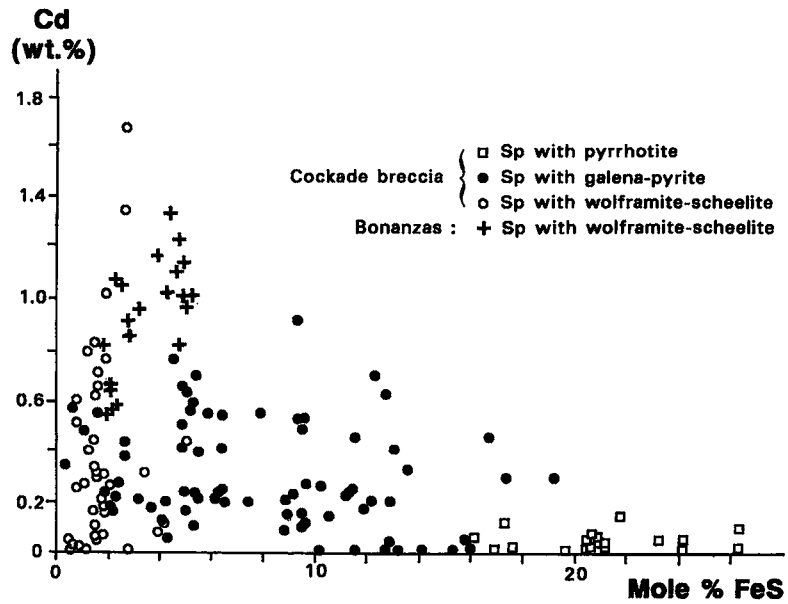


FIG. 11. Chemical composition of sphalerite from Cirotan. Results of electron-microprobe analyses (BRGM, CAMECA SX 50). Conditions of analysis: see Table 1.

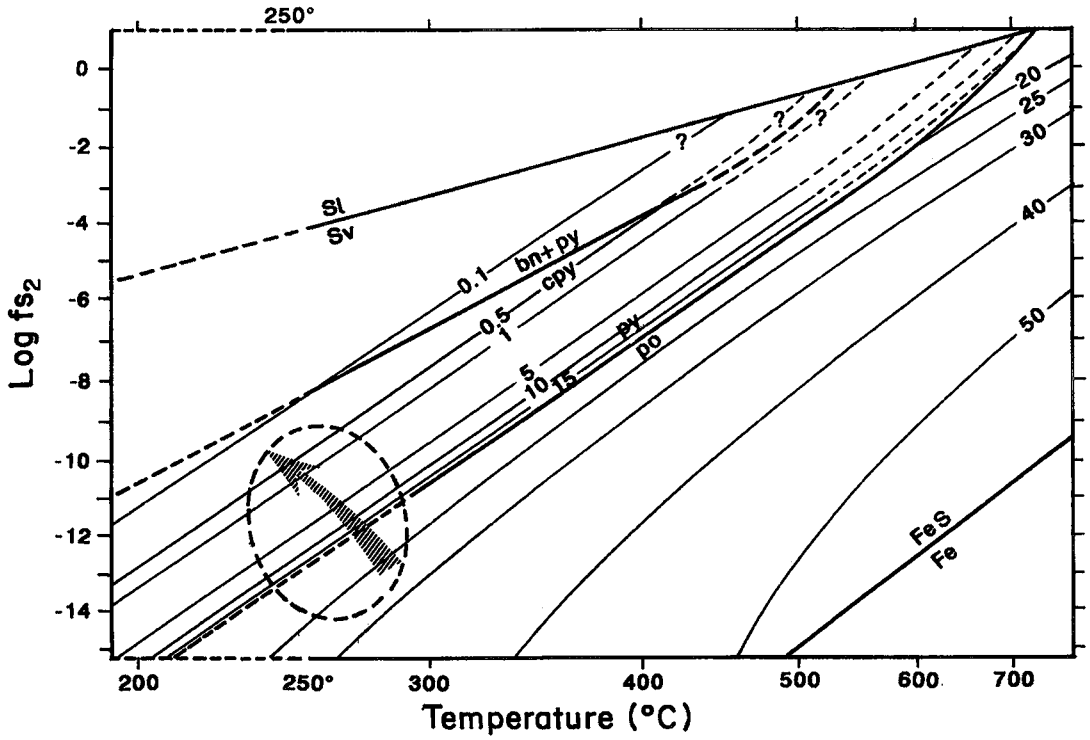


FIG. 12. Conditions of deposition of the sulfide paragenesis in the cockade breccias, in terms of temperature and fugacity of sulfur, showing the probable evolution within a sequence (arrow). Isopleths are mole % FeS in sphalerite coexisting with pyrrhotite or pyrite. Symbols: bn bornite, cpy chalcopyrite (or intermediate solid solution), po pyrrhotite, py pyrite, Sl liquid sulfur, Sv sulfur vapor. Pressure: 1 bar (after Scott 1983).

very risky, as has already been mentioned by many authors (Nakashima *et al.* 1986, Campbell & Petersen 1988).

Few data exist on the stability conditions of cassiterite at low temperatures (<300°C), although Grant *et al.* (1980) have shown that in some porphyry-tin deposits, cassiterite deposition could have taken place largely below 300°C. At this temperature, in the cassiterite–sulfide deposits, the stability conditions of cassiterite are broad, with $f(S_2)$ ranging from $10^{-10}$ to $10^{-15}$ atm, and $f(O_2)$ from $10^{-32}$ to $10^{-39}$ atm.

The $f(S_2)/f(O_2)$ diagram (Fig. 13) of Barton *et al.* (1977) enables the conditions to be narrowed down, taking into consideration that: 1) The iron content of the sphalerite immediately preceding the deposition of the cassiterite is low (2–5 mole % FeS), and 2) the stability field of the cassiterite can be considered to be more similar to that of magnetite than to that of hematite. Cassiterite–magnetite compatibility is, in fact, demonstrated by the equilibrium reactions in the tin-bearing Mg-rich skarns (Einaudi *et al.* 1981) and by the experimental results of Jiatu *et al.* (1988). The latter authors fixed the optimum physicochemical conditions for the formation of cassiterite–sulfide deposits in the Dachang ore field (China) at between 400 and 250°C, with an $f(O_2)$ of $10^{-28}$ to $10^{-40}$ atm.

The end of the bonanza stage occurred at lower $f(S_2)$ in the stability field of oxides, under conditions that can be estimated as $f(S_2)$ lower than $10^{-12}$ atm and $f(O_2)$ lower than $10^{-35}$ atm (Fig. 13). These conditions also prevailed, but very briefly, at the end of the cockade breccia stage, before a return to more reducing conditions (inter-cockades and beginning of the bonanzas). The low $f(S_2)$ conditions may have evolved during the deposition of the latest vuggy quartz and scheelite at the end of the process. The fluid inclusions trapped in this quartz indicate a clear lowering of temperature (212 to 159°C; Nehlig & Marcoux 1992).

Ferberite is only rarely in contact with pyrite or sphalerite, from which it is most commonly separated by a fringe of silica. This apparent corrosion of the sulfides by wolframite could reflect the appearance of more acidic conditions in the epithermal system, in the same way as it appeared at a relatively low tempera-

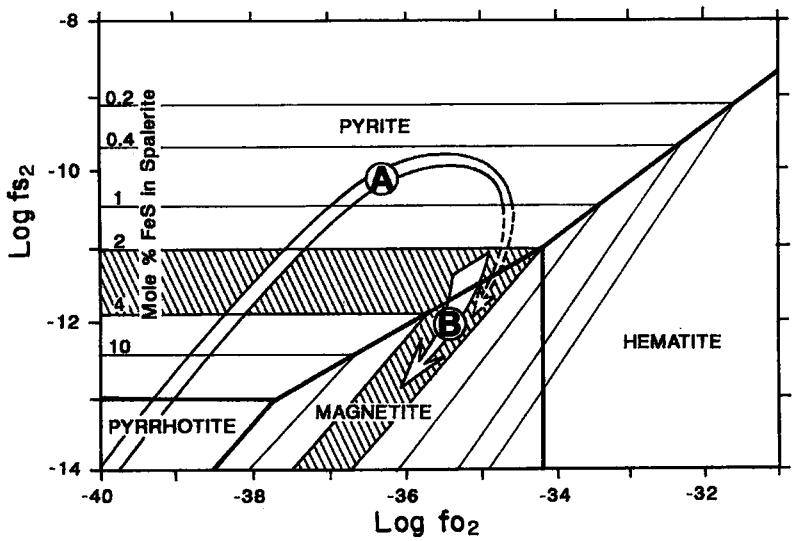


FIG. 13. Log $f(S_2)$ *versus* log $f(O_2)$ diagram at 250°C showing evolution of conditions of deposition for the cockade breccias (A) and precious brecciated ore (B). The shaded field corresponds to 2–5 mole % FeS in sphalerite cogenetic with wolframite–cassiterite. The field of stability of cassiterite can be assumed to be equivalent to that of magnetite. Quartz is present at all conditions shown. Diagram after Barton *et al.* (1977).

ture during the deposition of cassiterite in the skarns (Einaudi *et al.* 1981) and in the porphyry-tin deposits of Bolivia (Grant *et al.* 1980).

## Discussion and Conclusions

The Cirotan deposit possesses some of the usual textural and mineralogical characteristics of adularia–sericite epithermal deposits (Hayba *et al.* 1986, Berger & Bethke 1985, Heald *et al.* 1987, Ruvalcaba-Ruiz & Thomson 1988): banded and breccia textures, gangue of quartz – rhodochrosite – rhodonite – adularia – sericite, late enrichment in gold in the bonanzas. It also shows a certain number of unusual mineralogical features, the most unusual being the progressive appearance of cassiterite and ferberite, which become abundant in the bonanzas at the end of the depositional process, implying a shift to lower $f(S_2)$ conditions. The mineralogical evolution of deposits, with a late enrichment in gold, is well known but, to our knowledge, this is the first time that cassiterite also has been reported.

The composition of the cassiterite at Cirotan is characterized by high trace-element contents (3.2 wt.% FeO, 0.3 wt.% $Ta_2O_5$, 0.4 wt.% $In_2O_5$: Table 6). This particular composition has not been reported for cassiterite from various types of stanniferous deposit (Taylor 1979, Schneider *et al.* 1978, Moore & Howie 1979, Izoret *et al.* 1985, Giuliani 1987) and could be specific to this particular type of epithermal deposit, although earlier studies show a certain independence between the trace elements and the type of deposit, apart from granitic-pegmatite-related deposits.

The presence of tin in the hydrothermal solutions probably conditioned the appearance of Te-bearing canfieldite instead of hessite ($Ag_2Te$) or sylvanite [$(Au,Ag)_2Te_4$], which are normally associated with electrum in the bonanzas of epithermal deposits. This mineral appears, until now, to have been restricted to skarn-type and other granite-related Sn deposits (Soeda *et al.* 1984).

Ferberite began to appear in the last envelopes of the cockade breccias, and became abundant in the bonanzas, where it is intimately associated with cassiterite. Wolframite [$(Fe,Mn)WO_4$] is known, although only rarely, in epithermal deposits at Oatman (Arizona), Tonopah (Nevada), Julcani (Peru; Heald *et al.* 1987), and El Indio (Chile; Petersen *et al.* 1977, Siddeley & Araneda 1986), but in these deposits, hübnerite ($MnWO_4$) mostly is present. At Cirotan, it is of the ferberite variety which, along with the disappearance of rhodochrosite, indicates an exhaustion of manganese in the hydrothermal solutions.

Bismuth, a rare constituent in epithermal deposits, was only known in the acid-sulfate type of deposits, where it occurs in the form of bismuthinite ($Bi_2S_3$), and in a few adularia–sericite deposits, where it occurs in the form of aramayoite [$Ag(Bi,Sb)S_2$] (Marcoux & Milési, in press). At Cirotan, it is present in the form a Ag–Bi-rich lillianite; this mineral belongs to the uncommon gustavite–lillianite homeotypic series, whose rare minerals only are known from magma-

related mineralization at Tanco in Manitoba (Harris & Chen 1975), and La Roche-Balue in France (Moëlo *et al.* 1987), thus reinforcing the concept of a nearby magmatic source at Cirotan. Its presence is correlated with that of Sn and W. On the other hand, Mo is weak (maximum 108 ppm in the bonanzas) and seems to have no mineralogical expression.

The behavior of the gold is equally interesting. Most of the gold occurs in the form of electrum, but one observes an increase in the Au/Ag ratio with the evolution of the depositional process, combined with a noticeable increase in the size of the patches (from 0.5 μm in the cockade breccias to 230 μm in the bonanzas).

A gold sulfide, uytenbogaardtite, also appears in the bonanzas. This mineral, originally described in three localities (Barton *et al.* 1978), has since been observed at Orcopampa in Peru (Marcoux & Milési, in press), in the Bullfrog mining district, Nevada (Castor & Sjoberg 1993), and now at Cirotan. It appears to be specific to Cenozoic adularia–sericite epithermal deposits, where it is found in constant association with electrum and acanthite.

Among the other unusual features at Cirotan is a change in the mineralogical host of cadmium. This metal occurs in the form of Zn-bearing greenockite cogenetic with a Cd-poor sphalerite in the cockade breccia ore, but this pair of minerals disappears in favor of a cadmiferous sphalerite (as much as 2.2 wt.% Cd) on leaving the stability field of pyrite, *i.e.*, when the conditions became more oxidizing.

These mineralogical observations, associated with geochemical data on the ore, lead us to consider the Cirotan deposit as a hybrid type, transitional between a low-level adularia–sericite epithermal deposit and the porphyry-tin type deposits (Milési *et al.*, in press). Both the Sn–W contents and the lead isotope results ($^{207}Pb/^{204}Pb$ in the range 15.67–15.72) strongly suggest a reworking of the Precambrian continental crust underlying the Malaysia–Sumatra region for the source of the metals.

The hybrid nature of the Cirotan epithermal deposit, probably due to its proximal position to the magma source, enabled metals such as Sn, W and Bi (generally absent in epithermal deposits) to be expressed here, and thus explains the formation of an unusual assemblage of minerals. Other more classic elements, usually concentrated in the upper part of epithermal systems (Hg, Tl, Sb), are absent in the Cirotan paragenesis. These geochemical particularities accompany the noteworthy mineralogical features that make Cirotan and the West Java district a unique area of epithermal deposition of ore.

## Acknowledgements

The work for this article (BRGM contribution number 93008) was financially supported by a BRGM scientific programme (RM13b), investigating factors controlling gold deposits. The work was greatly helped in the field by the BRGM–DSM (Directorate of Sumberdaya Minerals, Bandung) cooperation team of the Ministry of Industry. Here, the authors give special thanks to K.A. Margawidjaja (Director of the DSM), A. Soedjarwadi & G. Faiman (Directors of Mines for the Cikotok district at Aneka Tambang), and Y. Sunarya (Chief of the Precious Metals Division, DSM). The authors are also grateful to the DSM and Aneka Tambang geologists and miners, particularly at the Cirotan mine, to their BRGM colleagues and to Y. Moëlo (CRSCM–CNRS Orléans), who provided valuable support, and to Sir Patrick Skipwith, Bt. and Dr. Marinus Kluyver for their translation of this contribution. This paper was considerably improved by two referees, whose help is gratefully acknowledged.

## References

Anthony, J.W., Bideaux, R.A., Bladh, K.W. & Nichols, M.C. (1990): *Handbook of Mineralogy* **1**. Mineral Data Publishing, Tucson, Arizona.

Barton, M.D., Kieft, C., Burke, E.A.J. & Oen, I.S. (1978): Uytenbogaardtite, a new silver–gold-sulfide. *Can. Mineral.* **16**, 651-657.

Barton, P.B., Jr., Bethke, P.H. & Roedder, E. (1977): Environment of ore deposition in the Creede Mining district, San Juan Mountains, Colarado. III. Progress toward interpretation of the chemistry of the ore-forming fluid for the OH vein. *Econ. Geol.* **72**, 1-24.

Berger, B.R. & Bethke, P.M. (1985): Geology and geochemistry of epithermal systems. *Rev. Econ. Geol.* **2.**

Campbell, A. & Petersen, U. (1988): Chemical zoning in wolframite from San Cristobal, Peru. *Miner. Deposita* **23**, 132-137.

Castor, S.B. & Sjoberg, J.J. (1993): Uytenbogaardtite, $Ag_3AuS_2$, in the Bullfrog mining district, Nevada. *Can. Mineral.* **31**, 88-98.

Claproth, R. (1989): Magmatic affinities of volcanic rocks from Ungaran, Central Java. *Geol. Indon.* **12**(1), 511-562.

Einaudi, M.T., Meinert, L.D. & Newberry, R.J. (1981): Skarn deposits. *Econ. Geol., 75th Anniv. Vol.*, 317-391.

Fouquet, Y., Auclair, G., Cambon, P. & Etoubleau, J. (1988): Geological setting and mineralogical and geochemical investigations on sulfide deposits near 13°N on the East Pacific Rise. *Marine Geol.* **84**, 145-178.

Genna, A. (1990): Etudes structurales des minéralisations aurifères épithermales, Ouest Java. *Bur. Rech. Géol. Minières, Rapp.* **R31226 GEO SGN 90.**

Giuliani, G. (1987): La cassitérite zonée du gisement de Sokhret Allat (granite des Zaër, Maroc Central): compo-

sition chimique et phases fluides associées. *Miner. Deposita* **22**, 253-261.

GOUANVIC, Y. & BABKINE, J. (1985): Métallogénie du gisement à tungstène–étain de Monteneme (N.W. Galice, Espagne). *Miner. Deposita* **20**, 8-15.

GRANT, J.N., HALLS, C., SHEPPARD, S.M.F. & AVILA, W. (1980): Evolution of the porphyry tin deposits of Bolivia. *Mining Geol., Spec. Issue* **8**, 151-173.

HARRIS, D.C. & CHEN, T.T. (1975): Gustavite: two Canadian occurrences. *Can. Mineral.* **13**, 411-414.

——— & OWENS, D.R. (1971): A tellurium-bearing canfieldite, from Revelstoke, B.C. *Can. Mineral.* **10**, 895-898.

HAYBA, D.O., BETHKE, P.M., HEALD, P. & FOLEY, N.K. (1985): Geologic, mineralogic, and geochemical characteristics of volcanic-hosted epithermal precious-metal deposits. *Rev. Econ. Geol.* **2**, 129-167.

HEALD, P., FOLEY, N.K. & HAYBA, D.O. (1987): Comparative anatomy of volcanic-hosted epithermal deposits: acid sulfate and adularia–sericite types. *Econ. Geol.* **82**, 1-26.

HSU, L.C. (1976): The stability relations of the wolframite series. *Am. Mineral.* **61**, 944-955.

IZORET, L., MARNIER, G. & DUSAUSOY, Y. (1985): Caractérisation cristallochimique de la cassitérite des gisements d'étain et de tungstène de Galice, Espagne. *Can. Mineral.* **23**, 221-231.

JIATU, Y., CHANGYI, C., JILIANG, Z. & YONGLIN, Z. (1988): Experimental research on the formation conditions of the cassiterite sulphide deposits in the Dachang tin ore fields. *In* Geology of Tin Deposits (C.S. Hutchinson, ed.). Springer Verlag, New York (373-382).

KARUP-MØLLER, S. (1970): Gustavite, a new sulphosalt mineral from Greenland. *Can. Mineral.* **10**, 173-190.

KATILI, J.A. (1975): Evolution of the Southeast Asian arc complex. *J. Indon. Assoc. Geol.* **21**(1), 113-143.

MACDIVITT, J.F. (1990): Overview of mineral development in Indonesia. *Geol. Indon.* **12**, 327-343.

MAKOVICKY, E. & KARUP-MØLLER, S. (1977): Chemistry and crystallography of the lillianite homologous series. II. Definition of new minerals: eskimoite, vikingite, ourayite and treasurite. Redefinition of schirmerite and new data on the lillianite–gustavite solid-solution series. *Neues Jahrb. Mineral. Abh.* **131**, 56-82.

MARCOUX, E. & MILÉSI, J.P. (1994): Mineralogical and textural position of Au–Ag bearing minerals in the evolution of the epithermal deposits of Orcopampa and Shila (Southern Peru). *Mineral and Petrol.*

MILÉSI, J.P., MARCOUX, E., NEHLIG, P., SUNARYA, Y., SUKANDAR & FELENC, J. (1994): Cirotan, West Java, Indonesia: a 1.7 m.y. hybrid epithermal Au–Ag–Sn–W deposit. *Econ. Geol.* (in press).

MOËLO, Y., MARCOUX, E., MAKOVICKY, E., KARUP-MØLLER, S. & LEGENDRE, O. (1987): Homologues de la lillianite (lillianite, vikingite, heyrovskyite riche en Ag et Bi...) de l'indice à W – As – (Pb, Bi, Ag) de la Roche Balue (Loire-Atlantique, France). *Bull. Minéral.* **110**, 43-64.

MOORE, F. & HOWIE, R.A. (1979): Geochemistry of some Cornubian cassiterites. *Miner. Deposita* **14**, 103-107.

MUROWCHICK, J.B. (1992): Marcasite inversion and the petrographic determination of pyrite ancestry. *Econ. Geol.* **87**, 1141-1152.

NAKASHIMA, K., WATANABE, M. & SOEDA, A. (1986): Regional and local variations in the composition of the wolframite series from SW Japan and possible factors controlling compositional variations. *Miner. Deposita* **21**, 200-206.

NEHLIG, P. & MARCOUX, E. (1992): Le gisement d'or épithermal de Cirotan (Ouest Java, Indonésie): contraintes microthermométriques. *C.R. Acad. Sci. Paris* **315**, *Sér.* **II**, 821-827.

PETERSEN, U., NOBLE, D.C., ARENAS, M.J. & GOODELL, P.C. (1977): Geology of the Julcani mining district, Peru. *Econ. Geol.* **72**, 931-949.

PICOT, P. & JOHAN, Z. (1983): Atlas of ore minerals (2nd edition). *Bur. Rech. Géol. Minières, Mém.* **90**.

ROEDDER, E. (1984): Fluid inclusions. *Rev. Mineral.* **12**.

RUVALCABA-RUIZ, D.C. & THOMPSON, T.B. (1988): Ore deposits at the Fresnillo mine, Zacatecas, Mexico. *Econ. Geol.* **83**, 1583-1596.

SCHNEIDER, H.J., DULSKI, P., LUCK, J., MÖLLER, P. & VILLALPANDO, A. (1978): Correlation of trace element distribution in cassiterites and geotectonic position of their deposits in Bolivia. *Miner. Deposita* **13**, 119-122.

SCOTT, S.D. (1983): Chemical behaviour of sphalerite and arsenopyrite in hydrothermal and metamorphic environments. *Mineral. Mag.* **47**, 427-435.

SHIMIZU, M. & SHIKAZONO, N. (1987): Stannoidite-bearing tin ore: mineralogy, texture and physicochemical environment of formation. *Can. Mineral.* **25**, 229-236.

SIDDELEY, G. & ARANEDA, R. (1986): The El Indio – Tambo gold deposits, Chile. *In* Proc. Gold '86 Symp., Toronto (445-456).

SOEDA, A., WATANABE, M., HOSHINO, K. & NAKASHIMA, K. (1984): Mineralogy of tellurium-bearing canfieldite from the Tsumo mine, SW Japan, and its implications for ore genesis. *Neues Jahrb. Mineral., Abh.* **150**, 11-23.

SUNARYA, Y. (1989): Overview of gold exploration and exploitation in Indonesia. *Geol. Indon.* **12**(1), 345-357.

TAYLOR, R.G. (1979): *Geology of Tin Deposits.* Elsevier, Amsterdam, The Netherlands.

VAN BEMMELEN, R.W. (1949): *The Geology of Indonesia* (2nd edition). Marinus Nijhoff, The Hague, The Netherlands.

WHITFORD, D.J., NICHOLLS, I.A. & TAYLOR, S.R. (1979): Spatial variations in the geochemistry of Quaternary lavas across the Sunda arc in Java and Bali. *Contrib. Mineral. Petrol.* **70**, 341-356.

WIMMERS, D. (1985): Silver minerals of Panasqueira, Portugal: a new occurrence of Te-bearing canfieldite. *Mineral. Mag.* **49**, 745-748.

*Received July 2, 1992, revised manuscript accepted February 12, 1993.*